PAPER

A novel method for determining water saturation of porous media in relative permeability measurement using DPT

View the article online for updates and enhancements.

A novel method for determining water saturation of porous media in relative permeability measurement using DPT

Shaicheng Shen[1,2] , **Zhiming Fang**[1,*] **and Xiaochun Li**[1]

[1] State Key Laboratory of Geomechanics and Geotechnical Engineering, Institute of Rock and Soil Mechanics, Chinese Academy of Sciences, Wuhan, Hubei 430071, People's Republic of China
[2] University of Chinese Academy of Sciences, Beijing 100049, People's Republic of China

E-mail: zmfang@whrsm.ac.cn

Abstract

Relative permeability is essential for understanding porous media's gas and water seepage characteristics and establishing production schedules in practical engineering applications. However, the movable water is too small to be detected in ultra-lowpermeability rocks, and it is difficult to determine the water saturation in the relative permeability measurement accurately. In this study, a differential pressure transducer (DPT) was applied to self-developed apparatus to quantify displaced water precisely. The results indicate that: (a) both the permeability and the relative permeability measurement results show high stability in repeatability tests with the application of DPT. (b) The final cumulative water flow data measured by the DPT is reliable; the relative error of the electronic balance and DPT value was less than 4%. (c) This self-developed instrument can obtain the relative permeability curve for ultra-low permeability rocks, such as tight sandstone and anthracite coal. Although there are limitations, this technique provides an economical and reliable pathway for studying the seepage characteristics of gas and water in ultra-low permeability rocks.

Keywords: porous media, relative permeability, water saturation, differential pressure transducer, ultra-low permeability rocks

(Some figures may appear in colour only in the online journal)

1. Introduction

Global warming is an important environmental issue in our society. Currently, many scientists are focusing on carbon reduction technologies, such as unconventional gas exploration [1], carbon capture and storage (CCS) [2, 3] and enhanced coalbed methane recovery (ECBM) [4, 5]. In these projects, the relative permeability of gas and water determines the wells' delivery capability when the two-phase flow is prevalent. However, for the unconventional reservoir, such as coal, tight sandstone and shale, it is difficult to determine the relative permeability data in the laboratory due to the low porosity and high irreducible water saturation of samples. Moreover, the pore closure behavior caused by adsorption-induced swelling decreases coal's permeability and relative permeability [6], further intensifying the difficulty in applying gas–water relative permeability measurement in coal.

Some scholars have developed devices to study the relative permeability curve in recent years to investigate gas–water flow characteristics in porous media. Dabbous *et al* [7] designed a device to study the effect of water on the flow behavior of methane in coals. The water was collected in a graduated fluid receiver tube. Durucan *et al* [8] developed similar relative permeability measurement apparatus. The separation tube was designed with a height of 1.5 m and an internal diameter of 25 mm to balance the measuring range and accuracy. We can intuitively observe the displaced water

in these devices. However, the gas–water interface becomes irregular and unstable as the gas flows through, which causes inaccuracies in water volume determinations [8]. In addition, an electronic balance was widely used in the past. Gash [9], Ham [10], Shen *et al* [11], Ge *et al* [12] and Zhang *et al* [13] quantified the displaced water by weighting the separation. The measurement accuracy of the balance is typically 0.001–0.01 g. However, the measurement error will be amplified due to the connection line between the separation unit and the core holder. With the development of new techniques, nuclear magnetic resonance (NMR) and x-ray computed tomography (CT) scanning were incorporated into the relative permeability measurement of porous media [14–18]. The water saturation can be obtained by T_2 data or imaged core slices. The visualization ability of these techniques allows us to observe the water distribution in the sample, which can help us further understand the displacement process in porous media. However, the sample size in these studies was limited due to the resolution of the equipment. It is uncertain whether the two-phase seepage characteristics of small-scale samples are similar to those of macroscopic samples. Moreover, x-ray CT or NMR techniques are more expensive than traditional volumetric and gravimetric techniques, which limits research on the relative permeability of ultra-low permeability rocks to some extent.

In this paper, a novel method was introduced to determine the water saturation of the sample when measuring the relative permeability. We combined a high-pressure separator and a high-precision differential pressure transducer (DPT). The amount of water in the gas–water separator can be recorded in real time by the DPT, and the water saturation of the sample can be inferred from the recorded data. Good performance has been demonstrated by a series of permeability and relative permeability repeatability tests. In addition, this device even demonstrates an excellent performance in the ultra-low permeability rocks' relative permeability measurement.

2. Apparatus

2.1. Apparatus composition

A schematic diagram and photograph of the relative permeability measurement apparatus are shown in figures 1 and 2, respectively. This novel apparatus enables absolute and relative permeability measurements under various pore and confining pressures. Two DPTs were applied in the apparatus. One was used to measure the differential pressure between upstream and downstream in permeability measurement using the pulse-decay technique. Another high-precision DPT was used to measure the accumulated water production in the separator.

The device can be divided into the following five parts according to its function: (a) fluid injection and control system; (b) control panel; (c) core clamping system; (d) gas–water separation system; (e) data acquisition system (DAQ).
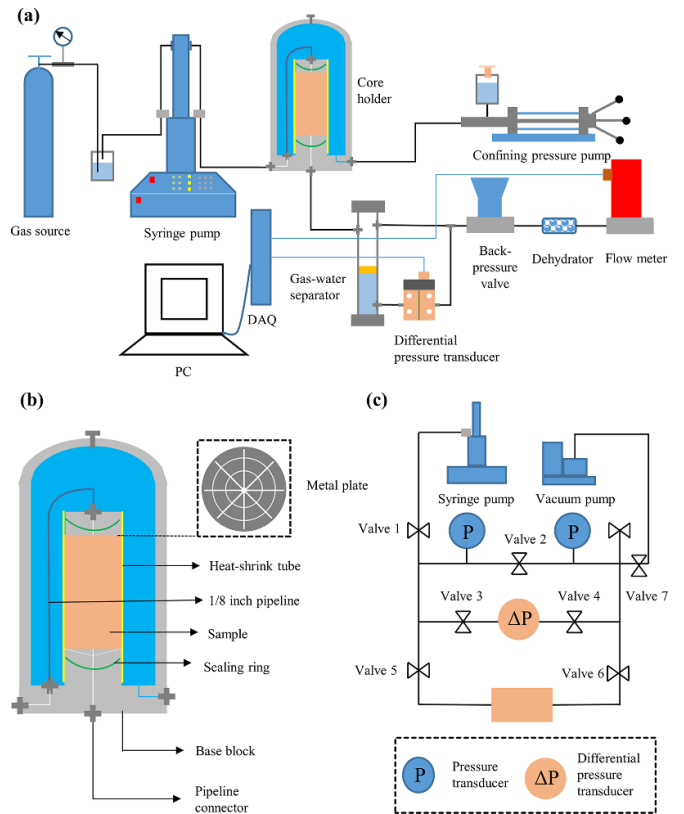

Figure 1. A schematic diagram of the self-developed device: (a) a structure diagram of the relative permeability measurement system; (b) a schematic of the core holder system; (c) a schematic of the permeability measurement unit of pulse decay.
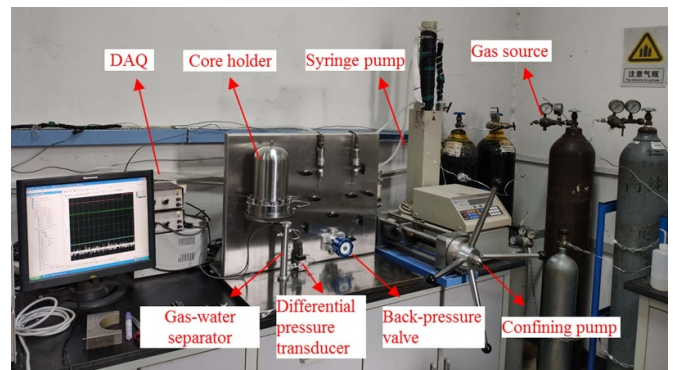
Figure 2. A photograph of the relative permeability measuring apparatus.

The fluid injection and control system includes a gas source, an ISCO pump and some pressure sensors. Helium, nitrogen, methane and carbon dioxide are included to meet various experimental requirements. The pressure range of the selected ISCO is 0.06895–68.95 MPa (68.95–68 950 kPa), and its measurement error is ±0.5% full scale (FS) under constant temperature conditions. Pressure sensors monitor the gas pressure in the pipeline in the range of 0–10 MPa. The measurement accuracy is 0.25% FS. Different gases can be stably

injected, controlled and monitored by this fluid control and injection system.

The control panel is mainly used to arrange the pipes and valves. When designing and installing, it is essential to ensure that the pipes and valves are arranged as symmetrically as possible. The arrangement of pipelines and valves is shown in figure 1(c). Valve 1 is connected to the pump, and it is the system's entrance. Valve 2 is a connection valve for upstream and downstream. It can help to quickly equalize the system pressure. Valves 3 and 4 are protective valves for the DPT to prevent it from being damaged. This DPT detects the pressure difference between upstream and downstream when measuring the permeability of porous media via the pulse-decay method or constant flow method. The measurement range and accuracy are 220 kPa and $\pm 0.25\%$ FS, respectively. Valves 5 and 6 are connected to the inlet and outlet of the core holder, respectively. Valve 7 is designed for convenient vacuuming.

The core clamping system comprises a core holder and a hand pump. The hand pump is the hydraulic pressure source to apply the confining pressure, and the maximum pressure is 25 MPa. The detailed construction of the core holder is shown in figure 1(b). The metal plate on the top and bottom of the sample is designed to ensure even injection and delivery of the fluid. The heat-shrink tube (0.5 mm thickness) and two sealing rings separate the sample from the confining liquid. The porous media and the pipeline are laid vertically from the end of the sample to the inlet of the separator to keep the amount of water remaining in the pipeline system as little as possible.

The gas–water separation system contains a gas–water separator, a DPT, a back-pressure valve, a dehydrator and a gas flow meter. The inner diameter of the gas–water separator is approximately 0.6 cm, and the height is approximately 20 cm. The separator is pre-installed with a small amount of water and oil to facilitate the calibration of the DPT and prevent the evaporation of water during the experiment. The DPT measurement range is -1.4 kPa to 1.4 kPa, and the accuracy is $\pm 0.25\%$ FS. The back-pressure valve is applied to maintain downstream pressure. A flow meter with a measuring range of 50 ml min^{-1} and accuracy of $\pm 0.5\%$ read data (RD)$+\pm 0.1\%$ FS was employed to measure the gas flow during the displacement process. A dehydrator was connected to the upstream of the flow meter to accurately and stably measure the gas flow rate.

The DAQ includes a computer, a data acquisition card, an universal serial bus (USB) - cable and some shielded cables. The data acquisition card has multiple acquisition channels, and we can simultaneously obtain all the sensor data, further improving the data collection capability. The text format data can be imported into an Excel sheet for data processing.

2.2. Main features and technical parameters

The device is designed, and we can easily operate it. This apparatus provides an effective method to study the characteristics of single-phase and gas–water two-phase flow in porous media. The main parameters of the device are as follows:

(a) The maximum confining pressure: 25 MPa;
(b) The maximum pore pressure: 10 MPa;
(c) The pressure range and accuracy of the syringe pump: 0.068 95 MPa to 25.86 MPa, with accuracy of $\pm 0.5\%$ FS at constant temperature;
(d) The measurement range and accuracy of the DPT: 220 kPa and 1.4 kPa, with accuracy of $\pm 0.25\%$ FS;
(e) The measurement range and accuracy of the flowmeter: 50 ml min^{-1}, with accuracy of $\pm 0.5\%$ RD$+\pm 0.1\%$ FS;
(f) Sample size: a cylindrical sample with a diameter of 50 mm and a height of less than 110 mm.

2.3. Test procedures

The unsteady-state method is usually applied to measure the relative permeability of porous media, and the test procedures are as follows:

(a) Sample preparation

Prepare a cylindrical sample with a diameter of 50 mm before the experiment due to the limitations of the core holder. The sample should be dried in a vacuum drying cabinet until the weight change is less than 0.1 g h^{-1}. Conduct the gas permeability test after drying; the test procedures are listed in a previous study [19]. Saturate the sample with water for 72 h after the permeability test. It is necessary to record the dried and water-saturated sample weight in time to calculate the initial porosity.

(b) Sample installation

Wrap the sample with a layer of silica gel to ensure the sample integrity and avoid surface-flow under low confining pressure. Then, jacket the sample using a heat-shrink tube to isolate it from confining fluid. Keep the metal plate in close contact with the sample to minimize the dead volume of the system and prevent the heat-shrink tube from being damaged.

(c) Loading of the confining pressure

Water was injected into the core holder as the confining fluid to apply hydrostatic pressure after the installation of the sample. The porosity will alter with the increase in confining pressure. Thus, the free water in the pores or cracks may be squeezed out from the sample. To minimize the effect of loading on the experiment, the loading rate was controlled by a hand pump with 0.05 MPa s^{-1}. Loading was stopped and the confining pressure was kept stable when it reached the designed value. The confining pressure may drop slightly due to the compression of the sample. We can manually compensate for the pressure loss.

(d) Gas injection and equilibrium

The back-pressure valve was set to a state before the gas injection. Thus, we can maintain the downstream pressure at the design value. Then, we injected the pore fluid into the system using a syringe pump. The syringe pump maintained the upstream pressure, and

the downstream was kept constant by a back-pressure valve during the test. It should be noted that large instantaneous pulses should be avoided due to the small range (−1.4 kPa to 1.4 kPa) and the sensitivity of the DPT.

(e) Displacement test

When the pore fluid pressure reaches the designed pressure, close the connection valves 2 and 5 (as shown in figure 1(c)) and then adjust the pump pressure to the design value to create a pulse pressure between the upstream and downstream. The applied pulse pressure can be evaluated according to the measurement results of the absolute permeability of the sample. Open valve 5 and record all the sensor readings in real time when the syringe pump flow rate is zero. The displacement test is considered to end if no water flow can be detected by the DPT. Take out the sample and weigh it again using an electronic balance.

(f) Data processing

The apparent permeability and relative permeability can be calculated according to the recorded data. Detailed calculation methods for the apparent permeability, absolute permeability and relative permeability are listed in appendix.

3. Verification and calibration

3.1. Tightness verification

The tightness of the pipe system needs to be examined before the experiment. An impermeable solid steel sample was placed into the core holder, and 5.1439 MPa nitrogen was injected into the pipe system for the tightness test. The temperature was maintained at $22 \pm 1\,°C$. The reading of the pressure sensors was continuously monitored for 21 h, and the results are shown in figure 3. The gas pressure reduced from 5.1439 MPa to 5.1395 MPa over 21 h. The leakage rate L_r can be defined by the pressure drop in the vessel:

$$L_r = -V\frac{\mathrm{d}P}{\mathrm{d}t} \tag{1}$$

where V is the volume of the vessel, m^3; P is the pressure, Pa; t is the time, s.

The leakage rate of the system is $1.229 \times 10^{-6}\,m^3\,Pa\,s^{-1}$. It is small and can be neglected in our experiments. The tightness of the pipe system meets the experiment requirements.

3.2. Pipe volume calibration

When passing the sealing performance inspection, the volume of the upstream and downstream was measured due to the application of the pulse-decay technique to determine the permeability. We divide the piping system into five parts, as shown in figure 4. Volume 1 represents the volume between valves 1, 2, 3 and 5; volume 2 represents the volume between valves 2, 4, 6, 7 and 8; volume 3 represents the volume between
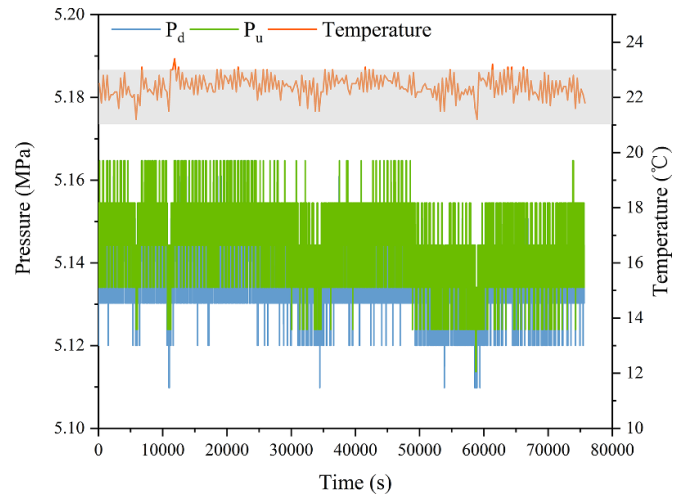

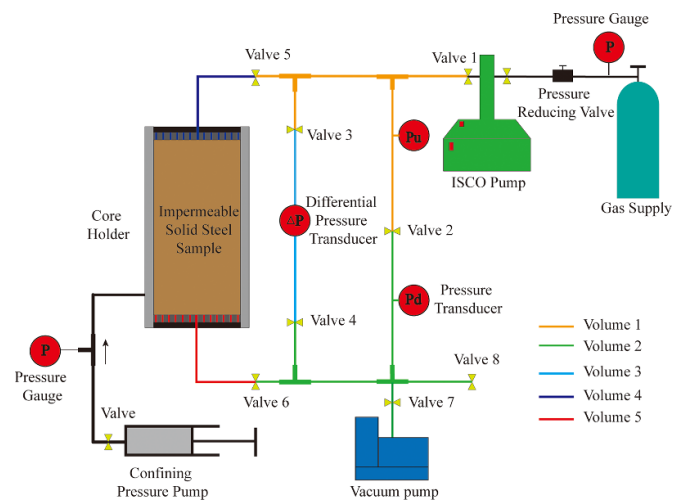**Figure 3.** Results of the leak test of the experimental system.

Figure 4. Division of the pipe volume and the measurement results.

valves 3 and 4; volume 4 represents the volume from valve 5 to the upside of the sample; volume 5 represents the volume from the downside of the sample to valve 6.

The ISCO pump measured each part's volume. The measurement procedures are as follows: (a) open all valves and vacuum; (b) close all valves; (c) inject 2 MPa nitrogen into the pump. Open valves 1, 2, 3, 4, 5 and 6 in order once the gas in the pump is stable. The volume change of the pump is equal to the corresponding pipe volume. The measurement results are shown in figure 5. The volume of upstream (V_u) and downstream (V_d) can be quantified, and the volumes are 11.13 ml and 9.99 ml, respectively.

3.3. Cumulative water determination by the DPT

The separator and the DPT are two essential parts of this self-developed apparatus. The accumulated water production
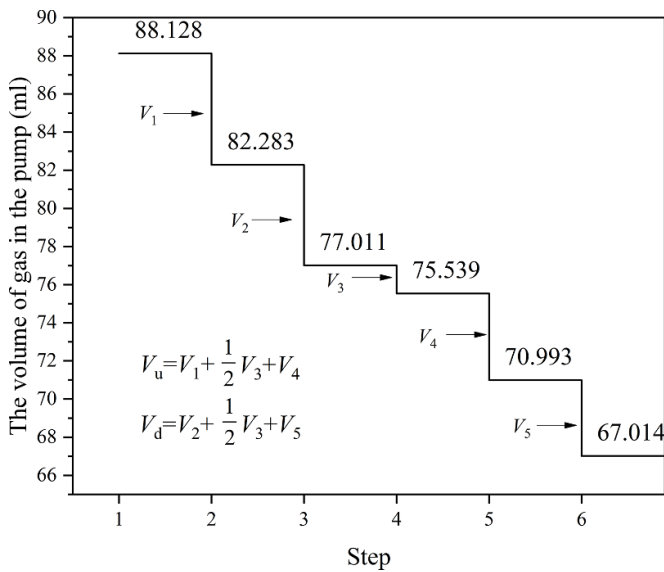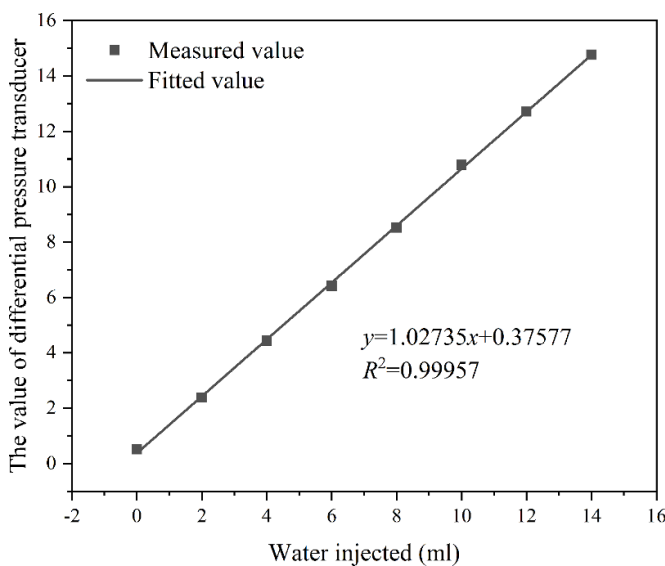
Figure 5. Pipeline volume measurement.

Figure 6. The relationship between the amount of water in the separator and the value of the DPT.

measurement is based on the liquid pressure formula ($p = \rho g h$). Therefore, the relationship between the amount of water and the value of the DPT is linear when the internal diameter of the separator is constant. Water is injected into the separator with a syringe seven times (2 ml each time). The relationship between the amount of water injected and the DPT value is shown in figure 6. It can be seen that the differential pressure increases by 1.027 35 when 1 ml of water is injected into the separator. We can determine the accumulated water from this relationship during the displacement process.

4. Measurement repeatability verification and measuring range tests

The measurement results' repeatability is an essential criterion for assessing the stability of the device. The cumulative water/gas production reflects each phase's flow rate, and the absolute permeability is the stretching factor for the relative permeability curve. Thus, both the cumulative gas/water production and the absolute permeability measurement repeatability were verified in this study. In addition, the device measurement limitation determines its application range. A series of experiments were performed on tight sandstone and coal to investigate its performance in ultra-low permeability rocks' relative permeability curve measurement.

4.1. Permeability tests' repeatability and measurement error determination

The constant flow and pressure methods are accurate and reliable for determining the permeability of intact cores in the laboratory if their permeability is greater than 1 mD. However, due to its shorter experimental times and higher resolution, the pulse-decay method was most applied to measure the permeability of low-permeability rocks. The repeatability of the measurement results for the constant flow method and pulse-decay method is verified in this work. Figure 7(a) shows the change in differential pressure in the sandstone permeability test using the constant flow method. Nitrogen was injected upstream at the rates of 20 ml min^{-1}, 10 ml min^{-1} and 10 ml min^{-1}, respectively. The final equalized differential pressure between upstream and downstream was 30.330 kPa, 14.548 kPa and 14.548 kPa. The gas permeability of sandstone can be calculated using equation (4), and the results are 11.20 mD, 11.07 mD and 11.07 mD, respectively. Figure 7(b) shows the differential pressure curve and corresponding data processing results obtained by pulse-decay technology during the coal permeability test. The gas permeability of coal can be calculated using equation (5), and the results are 5.56 μD, 5.49 μD and 5.45 μD, respectively. We evaluate the repeatability of this device by calculating the standard deviation of three permeability results. The standard deviation of the sandstone permeability is 0.0613, and that for coal is 0.0437. The tested permeability is stable, and this device performs well in permeability measurement.

4.2. Displacement tests' repeatability and measurement error determination

Considering the experiment's difficulty and duration, we decided to use sandstone for the displacement test to examine the repeatability of the self-developed device. In addition, the water production was determined by an electronic balance and a DPT, respectively, to determine the measurement error. Sandstone with a porosity of 12% was prepared to conduct a displacement test three times. The confining pressure, upstream pressure and downstream pressure are
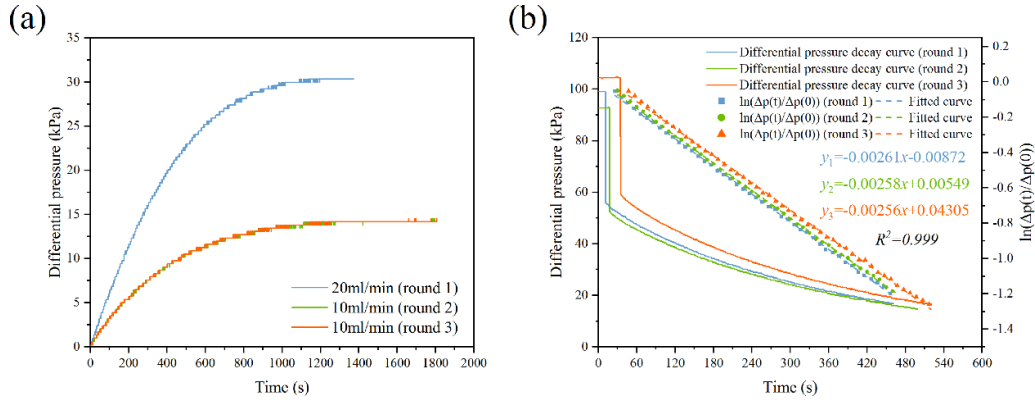
Figure 7. Results of the permeability tests. (a) Differential pressure variation in the permeability test using the constant flow method; (b) differential pressure variation during the permeability test with pulse-decay technology and corresponding data processing.

8.5 MPa, 0.25 MPa and 0.1 MPa, respectively. The test fluid is nitrogen, and the test procedures are described in section 2.3.

The repeatability test results are shown in figure 8. Figure 8(a) shows the water and gas cumulative production under atmospheric conditions. Figure 8(b) shows the volumetric flow rate. It can be observed that both of them show strong consistency in repeated experiments. Figure 8(c) illustrates the average and standard deviation of the cumulative gas and water production for three repeatability experiments. We define the global coefficient of variation (GCV) to quantitatively evaluate the stability of the measurement results. The GCV was calculated using equation (2):

$$\text{GCV} = \frac{1}{n}\sum_{i=1}^{n} \frac{\sqrt{\frac{1}{m}\sum_{j=1}^{m}\left(y_i^j - \bar{y}_i\right)^2}}{\bar{y}_i}. \tag{2}$$

The GCV for the accumulated water flow is 0.05, and that for the accumulated gas flow is 0.06. The repeatability of the displacement measurement results is acceptable for this self-developed device.

The final cumulative water production measured by the DPT was compared with that obtained by the electronic balance to verify the accuracy of the experimental results. The results are shown in figure 8(d). The relative error can be calculated using equation (3):

$$E_{\text{relative}} = \frac{m_w - m_{w}{'}}{m_w} \tag{3}$$

where m_w is the weight change of the rock sample before and after the displacement measured by the electronic balance, g; $m_{w}{'}$ is the amount of water measured by the DPT, g.

The quality of the water-saturated sandstone measured by the electronic balance is 463.47 g, 463.46 g and 463.26 g in three repeated tests, and it becomes 457.13 g, 457.12 g and 457.14 g after the displacement experiment. The final cumulative water production measured by the DPT is 6.219 g, 6.248 g and 5.924 g, respectively. The calculation results show that

the relative error of water production determined by the electronic balance and the DPT is less than 4%. This indicates that the water saturation of the sample can be reliably monitored with a DPT during the displacement process.

4.3. Measurement range tests

The displacement test in section 4.2 indicates that this self-developed device can measure the gas–water relative permeability of porous media with an absolute permeability of 11.11 mD and cumulative water of 6.2 ml. However, the lower the permeability and porosity, the higher the irreducible water saturation of the sample, and the more difficult it is to measure the relative permeability. Therefore, it makes more sense to determine the ultimate measurement capability of this device to obtain the relative permeability. Tight sandstone (with lower permeability) and anthracite coal (with lower permeability and high irreducible water saturation) were prepared for relative permeability measurement to verify the measuring range of the apparatus. The tight sandstone in this study was taken from Sichuan Province, China, containing 50.73% quartz, 34.01% albite, 10.59% calcite, 3.32% illite and 1.36% montmorillonite [20]. The anthracite coal sample was collected in coal seam #3 in the SiHe coal mine (in Shanxi Formation in the southern part of the Qinshui Basin), with 3.37% vitrinite reflectance, 79.84% vitrinite, 18.36% inertinite and 1.80% minerals [21]. The size of the intact cylindrical sample is 50 mm in diameter and 100 mm in length. Nitrogen was used as a displacing fluid for tight sandstone, and helium was used for coal to avoid matrix deformation induced by the adsorption effect [22–24]. The experiment conditions are shown in table 1. The test procedures are as described in section 2.3.

The gas and water cumulative production and relative permeability curves for tight sandstone are shown in figures 9(a) and (b). The water and nitrogen production show excellent continuity during the displacement, and the final accumulated water and nitrogen flow are 6.754 ml and 29 231.402 ml, respectively. The irreducible water saturation and water saturation at the cross-point are 40% and 62%, respectively. However, the relative permeability of tight sandstone is small
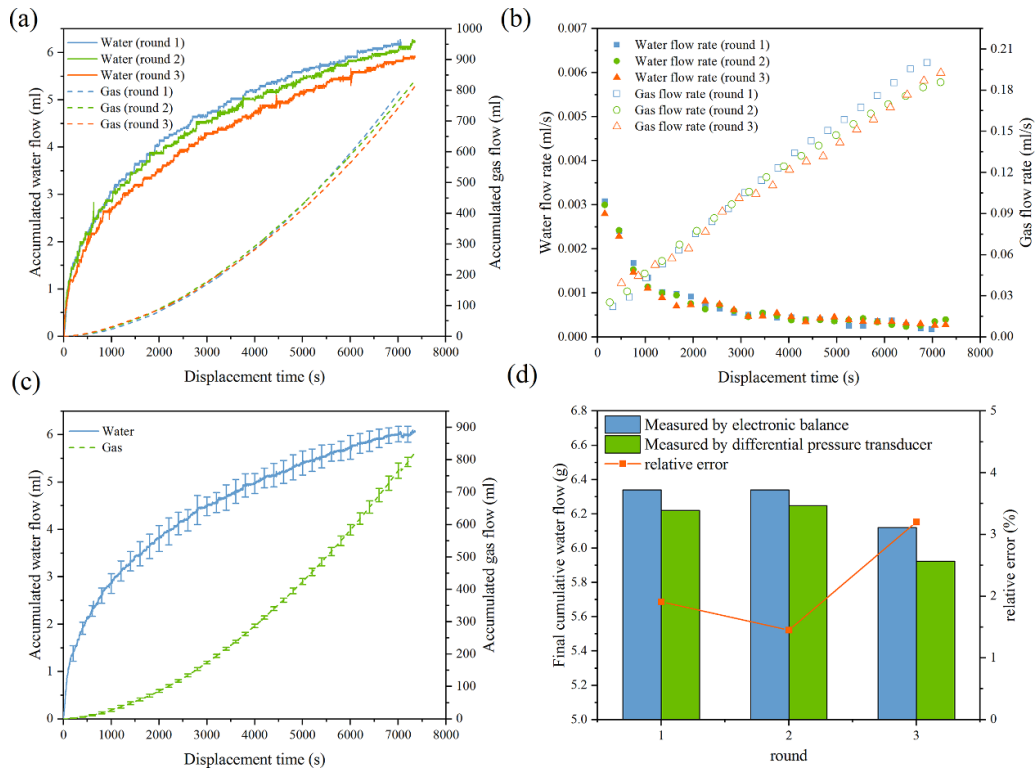
Figure 8. The results of the repeatability experiments. (a) Cumulative production of gas and water in the relative permeability test; (b) the 1st derivative of the cumulative production of gas and water; (c) the average and standard deviation of the cumulative production of gas and water for three repeatability experiments. (d) A comparison of cumulative water production measured by an electronic balance and a DPT.

Table 1. The experiment conditions for the relative permeability test.

Sample	Confining pressure/MPa	Upstream pressure/MPa	Downstream pressure/MPa	Porosity/%	Absolute permeability/μD
Tight sandstone	8	4.0	0.1	6.2	42.06
Coal	8.5	4.9	0.1	1.7	2.79

because the absolute permeability was measured with nitrogen and then corrected by the Klinkenberg equation [25]. In addition, some clay minerals (3.32% illite and 1.36% montmorillonite) are present in tight sandstone. The hydration expansion of clay minerals will reduce the effective pore throat and porosity upon contact with water, which causes lower permeability when measured by water rather than by gas [26, 27]. Therefore, the choice of absolute permeability causes a small relative permeability for both gas and water. The Brooks–Corey model [28] was used to fit the measured relative permeability, assuming that the porous media contained a bundle of capillary tubes with various radii. This assumption may correspond better to the structure of sandstone. The best-fitting value for the cleat size distribution index is 4.44.

The cumulative production of gas and water and relative permeability curves for anthracite coal are shown in figures 9(c) and (d). The final accumulated water and helium flows are 0.383 ml and 8912.538 ml, respectively. The relative permeability curve shows a narrow two-phase span, high irreducible water saturation and lower water relative permeability characteristics. These characteristics are consistent with the

high-rank coal (with a permeability less than 0.1 mD) relative permeability curve reported by Shen *et al* [29]. To evaluate the reliability of the relative permeability measurement using this self-developed device, we compared the measurement results with Sun *et al* [16]. A similar anthracite coal sample SH, which was from the same coal mine as the sample used in this study, was used for the relative permeability curve measurement in the research of Sun *et al* [16]. Their results show that the sample SH has extremely high irreducible water saturation (approximately 96%) and cross-point water saturation (about 99%). In addition, the relative permeability of water is lower compared with the gas phase. The maximum water and gas relative permeability is approximately 5% and 23%, respectively. These properties are similar to our measurements. The irreducible water saturation is 83.5%, and the cross-point water saturation is 99% in our study. The water and gas maximum relative permeability is 3% and 38%, respectively. The displacement pressure is 4.8 MPa in this study. However, the confining pressure is 4.3 MPa, and the net confining pressure is 3.5 MPa in the work of Sun, which means that the displacement pressure is less than 1.5 MPa. Some studies show that irreducible water saturation is related to displacement pressure
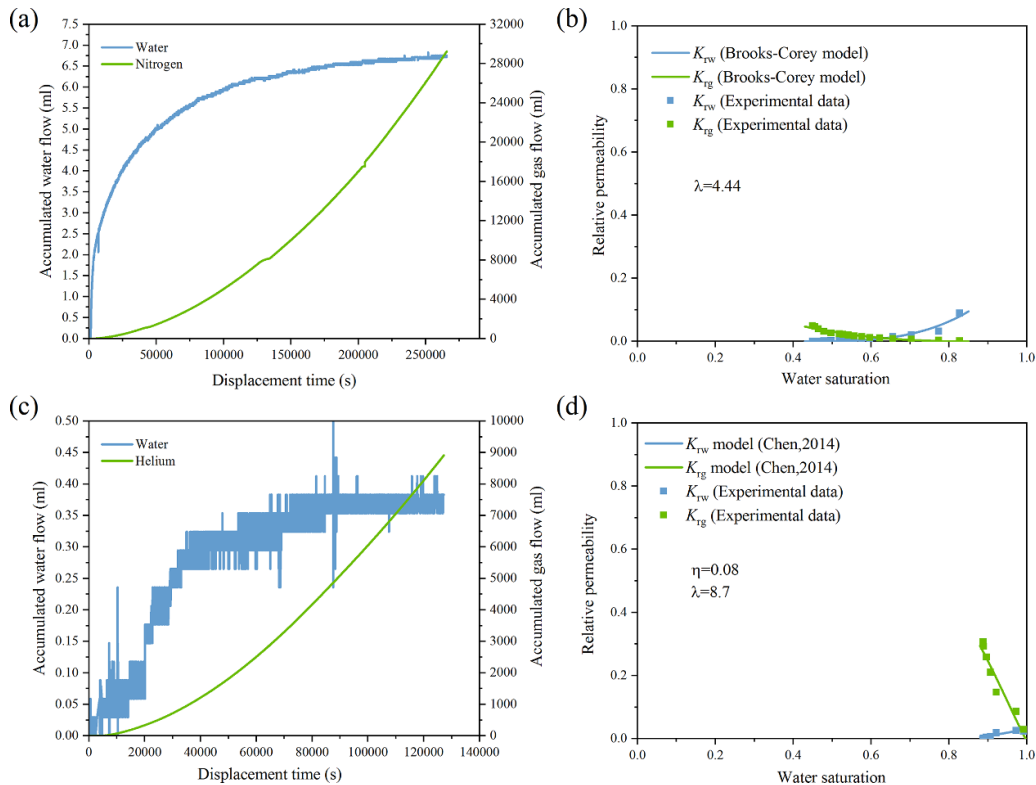
Figure 9. Results of the displacement experiments for tight sandstone and coal. (a) The accumulated water and gas flow for tight sandstone; (b) nitrogen–water relative permeability for tight sandstone; (c) the accumulated water and gas flow for coal; (d) helium–water relative permeability for coal.

[30–35]. Therefore, it is reasonable to consider that the difference in displacement pressure mainly causes the difference in irreducible water saturation in these two measurements. In general, these consistent results confirm the results from the self-developed device.

The matchstick geometry will better account for the seepage characteristics of coal due to the dual porosity structure. Therefore, the two-parameter model introduced by Chen *et al* [36] was applied to fit the measurement results via the least squares method. The best-fitting values for the cleat tortuosity parameter (η) and the cleat size distribution index (λ) are 0.08 and 8.7, respectively.

The above measurement results indicate that this device can measure the relative permeability of unconventional reservoirs with low porosity and permeability, such as coal and tight sandstone. The measurement limitation is mainly determined by the amount of water that can be displaced during the experiment. This apparatus can perform relative permeability experiments even if the cumulative water production is about 0.4 ml.

5. Discussion

5.1. Comparison of measurement techniques

The current techniques for determining water saturation in porous media mainly include gravimetric, volumetric and NMR/CT techniques. This chapter discusses the measurement accuracy, advantages and disadvantages of these measurement techniques.

The gravimetric technique was widely applied in the past. Many scholars [9–11] applied an electronic balance to measure the displaced water content during relative permeability measurement, but actual measurement error was not discussed in their papers. The cumulative water production in the studies of Ham [10] and Shen *et al* [11] is in the range of 2.7–25 ml and 0.7–1 ml, respectively. It is larger than the water production (about 0.4 ml) in our study. It is well known that an extensive-range electronic balance is required if the separation unit needs to withstand high pressures; therefore, the measurement accuracy is limited. It is necessary to solve the contradiction between its range and accuracy to improve the application of the gravimetric technique in relative permeability measurement. In addition, the connection line between the separation unit and the core holder usually causes an unstable electronic balance reading due to the pipeline's tensile stress, which will amplify the measurement error. For the volumetric technique, the fluctuating levels and manual readings can create uncertainty in the measurement results. As discussed in Durucan *et al* [8], the total error in measuring liquid menisci was approximately ±1.0 ml. This error is too large to measure the relative permeability of ultra-low permeability rock.

For NMR or CT techniques, the measurement accuracy of water saturation has not been clear until now because of the complexity of the influencing factor, such as sample characteristics, device resolution and even the model used for the data process [37]. In the NMR technique, the water content is proportional to the total amplitude of T_2 [16]. Thus, the

water measurement accuracy depends on the minimum of the total amplitude of T_2. As shown in Sun *et al* [16], the water content accuracy is 0.1 ml if the total amplitude of T_2 is up to 1×10^3 p.u. The wide application of NMR and CT is due to their advantage in visualization, which helps us to observe fluid distribution in porous media. However, due to their resolution, the sample size is limited in CT and NMR techniques. In the studies of Alexis *et al* [18] and Sun *et al* [16], the sample size is less than 5 cm, which cannot sufficiently represent the reservoir conditions.

The DPT technique is advantageous due to its adjustable measurement range with high precision and no sample size limitation. The measurement accuracy depends on the DPT accuracy and the designed inner diameter of the separator. As the inner diameter of the separation device decreases, the water measurement accuracy will increase, as shown in figure 10. To avoid surface capillary effects, we recommend that the inner diameter of the separation device is not less than 0.5 cm so that the minimum resolution of the device is less than ± 0.01 ml. The application conditions of the instrument are mainly determined by the moveable water content in the porous media. Suppose we define a data group with at least five data points as valid data. In this case, the device can measure the gas–water relative permeability of porous media as long as the moveable water content is more extensive than 0.05 ml.

5.2. Limitations and applications

In general, the ideal of measuring water production using a DPT is realized. This self-developed device shows high repeatability in permeability and displacement tests. In addition, the relative permeability measurements for tight sandstone and coal indicate that this apparatus can measure the relative permeability of unconventional reservoirs. However, there are some limitations to this instrument. First, the dead volume (the volume between the outlet surface of the sample and the inlet of the separator) is inevitable in the instrument. Thus, the moveable water may reside in the dead volume, even if the pipe is placed vertically, which adds extra inaccuracy to the accumulated water determination. In addition, the displaced water first converges in the dead volume. It then flows into the separator due to gravity and the pressure gradient during the displacement test; therefore, the measured water production time is hysteretic. Second, the temperature control system limits the application range of the device. The temperature ranges from 20 °C–25 °C in our study. However, the temperature is higher than 30 °C if the depth exceeds 1000 m [38]. Therefore, this instrument cannot carry out *in situ* relative permeability experiments. Third, the back-pressure control is inaccurate. It was found that the inherent breakthrough pressure of the back-pressure valve is up to 20 kPa. This means that the gas will accumulate downstream first. Only when the downstream pressure increases by about 20 kPa can the gas break through the back-pressure valve. Thus, the gas flow rate cannot be monitored immediately after gas breakthroughs.
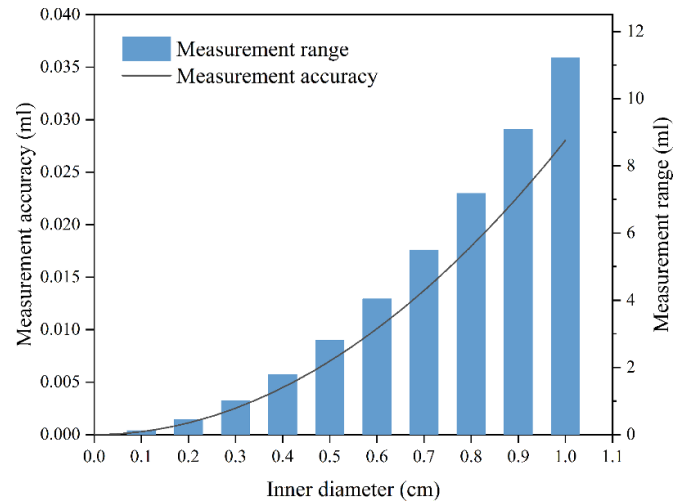

Figure 10. The relationship between the water content measurement range/accuracy and inner diameter of the separator.

Due to the difficulty in determining water saturation, the relative permeability measurement of ultra-low permeability rock was very limited in the past. Although uncertainties exist in this study, this study provides an effective method to evaluate the gas and water relative permeability characteristics of ultra-low permeability porous media. With this equipment, we can systematically study the influencing factors on relative permeability curves, which can help us to verify the applicability of the existing model and even establish new models. In addition, with the proposed concept of carbon neutrality, increasing numbers of CO_2-ECBM and CCS projects are waiting to be implemented. This device helps us to carry out carbon-dioxide–water or even mixed gas–water relative permeability tests in low-permeability rocks, which helps us to further understand the two-phase flow in the reservoir and provides reliable data for the simulation of CO_2-ECBM and CCS programs.

6. Conclusion

We designed special relative permeability measurement apparatus by combining the conventional unsteady method and the DPT technique. Both the permeability and relative permeability measurement results show excellent stability in the repeatability tests. By comparing the final water production measured by an electronic balance and a DPT, it was found that the relative error between them is less than 4%. The relative permeability measurement results indicate that this self-developed device can measure the relative permeability of ultra-low permeability rock, even if the accumulated water flow is approximately 0.4 ml. Compared with volumetric, gravimetric and NMR/CT techniques, the DPT is advantageous in its adjustable measurement range with high precision and no sample size limitations. Although there are some limitations with the apparatus, it is cheap, easy to operate and

has excellent stability, which makes it an effective way to study the relative permeability of porous media.

Data availability statement

The data that support the findings of this study are available upon reasonable request from the authors.

Conflict of interest

The authors declare that they have no conflicts of interest.

Author statement

Shaicheng Shen: conceptualization, methodology, investigation, writing—original draft; Xiaochun Li: formal analysis, supervision; Zhiming Fang: conceptualization, validation, writing—review and editing.

Appendix. Calculation of apparent permeability, absolute permeability and relative permeability

For the constant flow method, the apparent permeability (k_{app}) was calculated using equation (4) [39]:

$$k_{app} = -\frac{Q\mu_g L}{A}\frac{2p_d}{(p_d^2 - p_u^2)} \tag{4}$$

where Q is the flow rate, $m^3\ s^{-1}$; μ_g is the viscosity, Pa·s; L is the length of the sample, m; A is the section area of the sample, m^2; p_d is the outlet pressure, Pa; p_u is the inlet pressure, Pa.

For the pulse-decay method, the gas apparent permeability was calculated using equation (5) [40]:

$$k_{app} = \frac{-\alpha \mu_g L c_g}{f_1 A \left(\frac{1}{V_u} + \frac{1}{V_d}\right)} \tag{5}$$

where α is the slope of the decay curve in the semi-logarithmic plot, $1\ s^{-1}$; c_g is the gas compressibility, $1\ Pa^{-1}$; f_1 is the mass flow correction factor; V_u and V_d are the volumes of the upstream and downstream gas storage reservoirs, m^3.

To eliminate the gas slip effect, Klinkenberg-corrected permeability, which is also considered as the absolute permeability, can be determined using equation (6) [25]:

$$k_{app} = k_a \left(1 + \frac{b}{p_m}\right) \tag{6}$$

where k_a is the Klinkenberg-corrected permeability or absolute permeability of the sample, m^2; b is the Klinkenberg coefficient, Pa; p_m is the mean pore pressure, Pa.

The tight sandstone and anthracite coal apparent permeability and corresponding Klinkenberg-corrected permeability are shown in figure 11. The Klinkenberg-corrected permeability for tight sandstone and anthracite coal is 42.06 μD and 2.79 μD, respectively.

The relative permeability was calculated based on the cumulative production curve. Firstly, the recorded accumulated gas flow measured at the atmospheric pressure was corrected to that at the average pressure using equation (7):

$$V_{gi} = \frac{2p_a}{\Delta p + 2p_a} V'_{gi} \tag{7}$$

where V_{gi} is the corrected cumulative gas volume at the time point i, ml; V'_{gi} is the cumulative gas volume measured at the atmospheric pressure at the time point i, ml; p_a is the atmospheric pressure, MPa; Δp is the pressure difference between the upstream and downstream, MPa;

Then, the water and gas flow rate can be calculated using equations (8) and (9):

$$q_{wi} = \frac{1}{2}\left(\frac{V_{wi+1} - V_{wi}}{t_{i+1} - t_i} + \frac{V_{wi} - V_{wi-1}}{t_i - t_{i-1}}\right) \tag{8}$$

$$q_{gi} = \frac{1}{2}\left(\frac{V_{gi+1} - V_{gi}}{t_{i+1} - t_i} + \frac{V_{gi} - V_{gi-1}}{t_i - t_{i-1}}\right) \tag{9}$$

where q_{wi} and q_{gi} are the water and gas flow rate, respectively, $ml\ s^{-1}$; V_{wi} is the cumulative water volume at the time point i, ml; the subscripts $i-1$ and $i+1$ represent the time before and after time point i; t represents time, s.

Finally, the water saturation, gas and water relative permeability can be calculated using the Johnson, Bossler and Neumaann (JBN) method (equations (10)–(12)):

$$S_{wi} = \frac{V_p - V_{wi}}{V_p} \tag{10}$$

$$k_{rwi} = \frac{q_{wi}}{q_w} \tag{11}$$

$$k_{rgi} = k_{rwi} \cdot \frac{f_{gi}}{f_{wi}} \cdot \frac{\mu_g}{\mu_w} \tag{12}$$

where S_{wi} is the average water saturation, %; k_{rwi} is the water relative permeability, %; q_w is the water flow rate during single water phase flow, which is calculated by $q_w = \frac{AK}{\mu_w L}\Delta p$, $ml\ s^{-1}$; k_{rgi} is the gas relative permeability, %; f_{gi} is the fraction of gas, which is calculated by $f_{gi} = \frac{q_{gi}}{q_{wi}+q_{gi}}$, %; f_{wi} is the fraction of water, which is calculated by $f_{wi} = \frac{q_{wi}}{q_{wi}+q_{gi}}$, %; μ_w is the water viscosity, Pa·s.
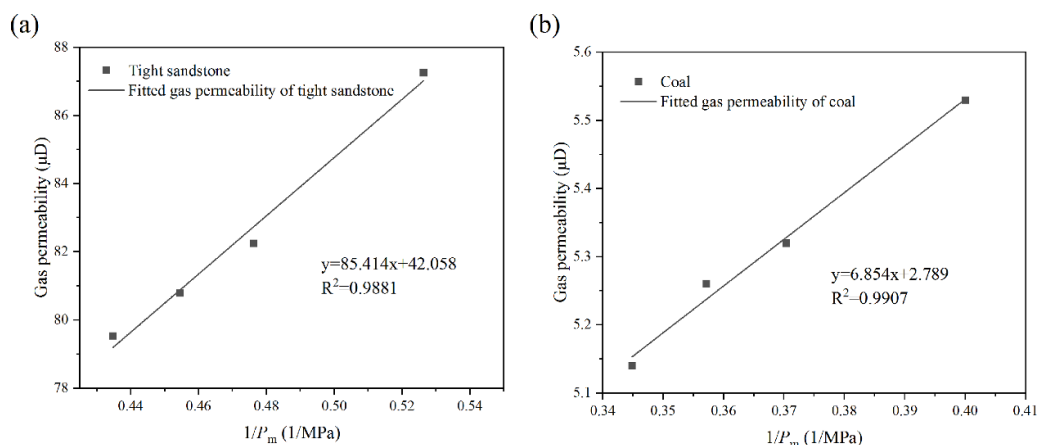
Figure 11. The apparent permeability and corresponding Klinkenberg-corrected permeability for tight sandstone and anthracite coal: (a) tight sandstone; (b) coal.

ORCID iD

Shaicheng Shen ⓘ https://orcid.org/0000-0003-3699-5305

References

[1] McGlade C, Speirs J and Sorrell S 2013 Unconventional gas—a review of regional and global resource estimates *Energy* **55** 571–84

[2] Mikunda T, Brunner L, Skylogianni E, Monteiro J, Rycroft L and Kemper J 2021 Carbon capture and storage and the sustainable development goals *Int. J. Greenh. Gas Control* **108** 103318

[3] Smit B 2016 Carbon capture and storage: introductory lecture *Faraday Discuss.* **192** 9–25

[4] Li Z B, Wei G M, Liang R, Shi P P, Wen H and Zhou W H 2021 LCO$_2$-ECBM technology for preventing coal and gas outburst: integrated effect of permeability improvement and gas displacement *Fuel* **285** 119219

[5] Hamza A, Hussein I A, Al-Marri M J, Mahmoud M, Shawabkeh R and Aparicio S 2021 CO$_2$ enhanced gas recovery and sequestration in depleted gas reservoirs: a review *J. Pet. Sci. Eng.* **196** 107685

[6] Zhou Y, Guan W, Cong P and Sun Q 2022 Effects of heterogeneous pore closure on the permeability of coal involving adsorption-induced swelling: a micro pore-scale simulation *Energy* **258** 124859

[7] Dabbous M K, Reznik A A, Taber J J and Fulton P F 1974 The permeability of coal to gas and water *Soc. Pet. Eng. J.* **14** 563–72

[8] Durucan S, Ahsan M, Shi J Q, Syed A and Korre A 2014 Two phase relative permeabilities for gas and water in selected European coals *Fuel* **134** 226–36

[9] Gash B W 1991 Measurement of "rock properties" in Coal for Coalbed Methane Production *SPE Annual Technical Conf. and Exhibition, Society of Petroleum Engineers* pp 221–30

[10] Ham Y 2011 Measurement and simulation of relative permeability of coal to gas and water *PhD Thesis* The University of Calgary (https://doi.org/10.11575/PRISM/4104)

[11] Shen J, Qin Y, Li Y P and Wang G 2019 Experimental investigation into the relative permeability of gas and water in low-rank coal *J. Pet. Sci. Eng.* **175** 303–16

[12] Ge L, Soares F T, Mahoney S, Hamilton C, Khan C, Steel K, Rufford T E and Rudolph V 2019 Effect of oxidation and silane surface treatments of coal powders on relative permeability in packed coal beds *J. Nat. Gas Sci. Eng.* **69** 1–9

[13] Zhang Z, Yan D, Yang S, Zhuang X, Li G, Wang G and Xiaoming W 2020 Experimental studies on the movable-water saturations of different-scale pores and relative permeability of low-medium rank coals from the Southern Junggar Basin *J. Nat. Gas Sci. Eng.* **83** 103585

[14] Zhao H P, Hu J H, Wang J K and Zhang Y 2019 A comprehensive model for calculating relative permeability based on spontaneous imbibition and CT scanning measurement *Fuel* **247** 287–93

[15] Schembre J M and Kovscek A R 2003 A technique for measuring two-phase relative permeability in porous media via x-ray CT measurements *J. Pet. Sci. Eng.* **39** 159–74

[16] Sun X, Yao Y, Ripepi N, Liu D and Novel A 2018 Method for gas-water relative permeability measurement of coal using NMR relaxation *Transp. Porous Media* **124** 73–90

[17] Shikhov I, d'Eurydice M N, Arns J Y and Arns C H 2017 An experimental and numerical study of relative permeability estimates using spatially resolved T_1-z NMR, transport in porous media **118** 225–50

[18] Alexis D A, Karpyn Z T, Ertekin T and Crandall D 2015 Fracture permeability and relative permeability of coal and their dependence on stress conditions *J. Unconv. Oil Gas Res.* **10** 1–10

[19] Shen S C, Li X C, Fang Z M and Shen N A 2020 Effect of gas adsorption on the application of the pulse-decay technique *Geofluids* **2020** 8872888

[20] Zhang Q, Li X, Bai B and Hu H 2019 The shear behavior of sandstone joints under different fluid and temperature conditions *Eng. Geol.* **257** 105143

[21] Han S J, Sang S X, Liang J J and Zhang J C 2019 Supercritical CO$_2$ adsorption in a simulated deep coal reservoir environment, implications for geological storage of CO$_2$ in deep coals in the southern Qinshui Basin, China *Energy Sci. Eng.* **7** 488–503

[22] Fang Z M, Li X C and Huang L 2013 Laboratory measurement and modelling of coal permeability with different gases adsorption *Int. J. Oil Gas Coal Technol.* **6** 567–80

[23] Robertson E P and Christiansen R L 2005 Measurement of sorption-induced strain (Idaho National Laboratory (INL))

[24] Kelemen S, Kwiatek L and Lee A 2006 *Swelling and Sorption Response of Selected Argonne Premium Bituminous Coals to CO$_2$, CH$_4$, and N$_2$, Int. CBM Symp.* (Tuscaloosa, Alabama)

[25] Klinkenberg L J 1941 The permeability of porous media to liquids and gases, drilling and production practice (New York: American Petroleum Institute) pp 200–13

[26] Faulkner D R and Rutter E H 2000 Comparisons of water and argon permeability in natural clay-bearing fault gouge under high pressure at 20 degrees C *J. Geophys. Res.* **105** 16415–26

[27] Duan Q B, Chen J Y and Yang X S 2020 A comparison of gas and water permeability in clay-bearing fault and reservoir rocks: experimental results and evolution mechanisms *J. Geophys. Res.* **125** e2019JB018278

[28] Brooks R H and Corey A T 1966 Properties of porous media affecting fluid flow *J. Irrig. Drain. Div.* **92** 61–88

[29] Shen S C, Fang Z M and Li X C 2020 Laboratory measurements of the relative permeability of coal: a review *Energies* **13** 5568

[30] Dai J Y, Wang J, Kong M, Zhang H X and Li Z L 2016 Dynamic irreducible water saturation and its determination method *3rd Int. Conf. on Material Engineering and Application (ICMEA)* (Shanghai) pp 415–9

[31] Yang M F, Yang Z B, Sun B, Zhang Z G, Liu H L and Zhao J L 2020 A study on the flowability of gas displacing water in low-permeability coal reservoir based on NMR technology *Front. Earth Sci.* **14** 673–83

[32] Mo S Y, He S L, Lei G, Gai S H and Liu Z K 2015 Effect of the drawdown pressure on the relative permeability in tight gas: a theoretical and experimental study *J. Nat. Gas Sci. Eng.* **24** 264–71

[33] Gao S S, Ye L Y, Xiong W, Zhong B, Yang H Z, Hu Z M, Liu H X and Xue H 2013 Seepage mechanism and strategy for development of large and low permeability and tight sandstone gas reservoirs with water content *J. Oil Gas Technol.* **35** 93–99

[34] Ping G, Weigang H and Yiwei J 2006 Research on the irreducible and movable water of tight sandstone gas reservoir *Nat. Gas Ind.* **26** 99–101

[35] Cheng Y, Zhang C and Zhu L Q 2017 A fractal irreducible water saturation model for capillary tubes and its application in tight gas reservoir *J. Pet. Sci. Eng.* **159** 731–9

[36] Chen D, Shi J Q, Durucan S and Korre A 2014 Gas and water relative permeability in different coals: model match and new insights *Int. J. Coal Geol.* **122** 37–49

[37] Shen J, Qin Y, Wang G X, Fu X H, Wei C T and Lei B 2011 Relative permeabilities of gas and water for different rank coals *Int. J. Coal Geol.* **86** 266–75

[38] Shen J, Qin Y, Zhang C, Hu Q and Chen W 2016 Feasibility of enhanced coalbed methane recovery by CO_2 into deep coalbed of Qinshui Basin *J. China Coal Soc.* **41** 156–61

[39] Chen G 1994 Gas slippage and Matrix Shrinkage Effects on Permeability of Coal *PhD Thesis* The University of Arizona pp 115–8

[40] Jones S C 1997 A technique for faster pulse-decay permeability measurements in tight rocks *SPE Formation Eval.* **12** 19–25